STUDY OF THE PROPAGATION CHARACTERISTICS OF CERTAIN MICROWAVE LINKS IN BRITISH COLUMBIA

Final Report

By: M. Kharadly (Principal Investigator)

For: Department of Communications, Ottawa, Canada

Under: Department of Supply and Services Contract
Serial Number OSV82-00018

Period: April 1, 1982 to March 31, 1983

DEPARTMENT OF ELECTRICAL ENGINEERING
FACULTY OF APPLIED SCIENCE
THE UNIVERSITY OF BRITISH COLUMBIA

P
91
C655
K54
1983
v.5

P
91
C655
K54
1983
V.5

DD 4830257
DL 4830444

checked 11/8 Queen
P
91
C655
K54
1983
v.5

Study of the Propagation Characteristics of Certain Microwave Links in British Columbia

The work under Contract No. OSV82-00018 is primarily concerned with the analysis of data obtained on various microwave links in British Columbia. This report consists of two parts. The first deals essentially with the effect of the melting layer on analog and digital transmission, using data obtained on the Hope-Chilliwack link. The second part is an analysis of data obtained on twelve links in representative regions of the Province, with regard to multipath effects.

The cooperation and assistance of the British Columbia Telephone Company is performing the work are gratefully acknowledged.

COMMUNICATIONS CANADA
OCT 12 1984
LIBRARY – BIBLIOTHÈQUE

Industry Canada
Library Queen
JUIL JUL 2 1 1998
Industrie Canada
Bibliothèque Queen

Part I: Observations of Abnormal Microwave Propagation Phenomena During Melting-Layer Conditions.

By: M. Kharadly, N. Owen, J. Van der Star, D. Michelson and T. Enegren.

To be presented at the Third International Conference on Antennas and Propagation, ICAP 83, University of East Anglia, Norwich, U.K., 12-15 April, 1983.

OBSERVATIONS OF ABNORMAL MICROWAVE PROPAGATION PHENOMENA DURING MELTING LAYER CONDITIONS

M. Kharadly*, N. Owen**, J. Van der Star*, D. Michelson*, and T. Enegren*

*University of British Columbia, Canada
**British Columbia Telephone Company, Canada

INTRODUCTION

Many investigators, including Watson (1), Oomari and Aoyagi (2), Austin (3), and Van der Star and Kharadly (4), have reported that the presence of a melting layer in a propagation channel increased the channel attenuation above that which could be attributed to rain. This paper presents, in addition to observations depicting severe cases of this phenomenon, other anomalous fading phenomena that were associated with the presence of the melting layer. These observations were made on a microwave slant path in British Columbia approximately 200 km inland from the Pacific Ocean.

The Path

The path is 41.3 km long with a 1227 m elevation differential. The path profile is shown in Figure 1. With the 1.7° elevation angle of this path, and using a thickness of the melting layer of 400 m (as observed by Dissanayake and McEwan (5)), the microwave beam will propagate in the melting layer for approximately 15 km, or slightly more than one-third of the path's total length.

The path's rather large elevation differential increases the probability that the zero degree isotherm will intersect the beam during the winter season.

Scope

Four analog channels in the 4 and 7 GHz bands (part of the Trans-Canada Telephone System microwave network) were monitored. A digital channel (91 Mb/s capacity) in the 8 GHz band that used vertical polarization was also monitored. The digital radio used vertical space diversity with dual receivers and a slope adaptive equalizer as protection against multipath fading. A description of this radio was given by DeWitte (5). A second digital channel, of orthogonal polarization and offset by 21 MHz, was used to study the feasibility of cross-polar frequency re-use on this path. The major characteristics of all radios are given in Table 1. The antenna arrangement at the transmitter and receiver sites is shown in Figure 2.

Data Acquisition

The data presented in this paper were collected during two different experiments conducted simultaneously by the University of British Columbia (UBC) and the British Columbia Telephone Company (B.C. Tel). The analog radio signal levels received at Ryder Lake and several meteorological parameters at stations along the path (Figure 1) were sampled and recorded by UBC's microprocessor based data acquisition system. UBC's monitoring system was described by Van der Star and Kharadly (4). The digital radio was monitored by B.C. Tel using a Datalog microcomputer developed by the Communications Reserach Centre, Ottawa. The digital radio parameters were also recorded (with lower resolution) on a chart recorder. A list of the parameters recorded by the combined systems is presented in Table 2.

OBSERVATIONS

Four abnormal propagation phenomena were observed during the 1981/82 winter season:

a. excessive attenuation;

b. abrupt changes in channel attenuation;

c. anomalous polarization dependence of channel attenuation; and

d. anomalous frequency dependence of channel attenuation.

TABLE 1 - Characteristics of the microwave radio equipment monitored at Ryder Lake

Frequency (GHz)	Polarization	Occupied Bandwidth (MHz)	Modulation	Free Space Received Signal Level (dBm)	Threshold (dBm)	Antenna Gain Transmit (dB)	Antenna Gain Receive (dB)
3.550	Horizontal	20	FM,FDM	-28.0	-69.5	39.0	39.0
4.010	Vertical	20	FM,FDM	-32.0	-68.5	40.1	40.1
7.142	Horizontal	20	FM,FDM	-40.5	-65.5	44.2	44.2
7.496	Horizontal	20	FM,FDM	-41.0	-69.5	44.5	44.5
7.765	Horizontal	40	QPRS,TDM	-24.5	--	45.3	45.3 main 44.9 div.
7.786	Vertical	40	QPRS,TDM	-24.0	-72.5	45.3	45.3 main 44.9 div.

Notes: 1. Analog threshold to squelch (mute).
2. Digital threshold to 10^{-4} BER.

TABLE 2 - List of propagation parameters recorded by UBC and B.C. Tel

Parameter	Sampling Frequency (Hz)
ANALOG RADIO RECEIVED SIGNAL LEVELS:	
3.550 GHz	10.0
4.010 GHz	10.0
7.142 GHz	10.0
7.496 GHz	10.0
DIGITAL RADIO RECEIVED SIGNAL LEVELS:	
7.765 GHz interference channel	10.0
7.786 GHz main receiver	10.0
7.786 GHz diversity receiver	10.0
7.786 GHz combined channel	10.0
DIGITAL RADIO PERFORMANCE PARAMETERS:	
Adaptive Equalizer Slope	10.0
Eye Voltage	10.0
Bit Error Rate	1.0
METEOROLOGICAL PARAMETERS:	
Ryder Lake Temperature	1.0
Rain Rate	1.0
Wind Speed	1.0
Wind Direction	1.0
Agassiz Temperature	1.0
Rain Rate	1.0
Wind Speed	1.0
Wind Direction	1.0
Dog Mtn. Temperature	1.0
Rain Rate	1.0

Excessive Attenuation

Fading greater than could be attributed to rain attenuation was observed on several occasions. As stated above, this effect has been previously reported (1) (2) (3) (4). Following (4), we describe the excessive attenuation by an "Excess Attenuation Ratio", EAR.

$$EAR = \frac{\text{excess attenuation due to melting layer (dB/km)}}{\text{basic attenuation due to rain, assuming Laws and Parsons distribution at 0°C (dB/km)}}$$

One of the events that was analyzed for excess attenuation is shown in Figure 3. The results for several events are presented in Table 3.

Abrupt Changes in Channel Attenuation

Abrupt changes in signal level were observed, both upwards and downwards. The former were more common. During one event, shown in Figure 4, the received signal level decreased 15 dB at a rate of 16 dB/s. One minute, twenty seconds later, it increased 20 dB at a rate of 30 dB/s. Such abrupt changes in received signal strength were not confined to one frequency or polarization, but were frequently observed simultaneously on signals within the same band, as shown in Figure 5.

It was also observed that these abrupt changes in channel attenuation occurred at or near times when certain weather parameters also changed suddenly. Figure 6 shows an expanded portion (twenty minute interval) of the event shown in Figure 5. During this interval, the 4 GHz signal level increased by 10 dB in less than one minute while the 7 GHz signal level

TABLE 3 - Excess attenuation ratios for several melting layer events

Date of Event	Sample Number	Channel Frequency (GHz)	Average Rain Rate (mm/hr)	Average Attenuation				Excess Attenuation Ratio
				Measured (dB)	Rain (dB)	Rain (dB/km)	Melting Layer (dB/km)	
1982-01-23	1	7.496	4.4	8.8	1.5	0.036	0.51	14
1982-01-23	1	7.786	4.4	15.0	1.5	0.036	0.94	26
1982-01-23	2	7.496	4.4	7.8	1.5	0.036	0.44	12
1982-01-23	3	7.496	3.5	7.1	1.1	0.027	0.42	16
1982-01-23	4	7.496	4.4	6.9	1.5	0.036	0.37	10
1982-01-23	5	7.496	1.3	3.0	0.4	0.009	0.18	19
1982-02-19	1	4.010	0.6	0.6	0.04	0.001	0.044	40
1982-02-19	1	7.496	0.6	1.5	0.17	0.004	0.092	22
1982-02-19	2	4.010	4.0	1.6	0.2	0.005	0.097	20
1982-02-19	2	7.496	4.0	6.0	1.36	0.033	0.321	10
1982-02-19	3	4.010	11.2	2.5	0.57	0.014	0.134	10
1982-02-19	3	7.496	11.2	8.5	4.50	0.111	0.277	3
1982-02-19	4	4.010	9.0	2.4	0.45	0.011	0.135	12
1982-02-19	4	7.496	9.0	6.5	3.50	0.086	0.208	2
1982-02-19	5	4.010	4.0	1.0	0.20	0.005	0.056	11
1982-02-19	5	7.496	4.0	3.0	1.36	0.033	0.114	3
1982-02-19	5	7.786	4.0	8.0	1.36	0.008	0.114	14
1982-02-19	6	4.010	1.2	0.7	0.06	0.0015	0.044	31
1982-02-19	6	7.496	1.2	3.7	0.36	0.009	0.229	27

Note: Average values of attenuation attributed to rain are calculated values based on Laws and Parsons distribution at 0°C.

increased abruptly four times in steps of about 5 dB each, before decreasing suddenly by a step of 5 dB. It is interesting to note that the wind speed and direction at Ryder Lake (the receiver site) also changed suddenly at about the same time, as shown in Figure 6.

Anomalous Polarization Dependence of Channel Attenuation

This was not very evident in the 4 GHz band but was quite apparent in the 8 GHz band. One example of this is shown in Figure 5, where the 7.765 GHz cross-polar interference signal level increased abruptly approximately twenty minutes after the 7.786 GHz signal levels did.

During other melting layer events, loss of cross-polar discrimination resulted in eye closure and a significant bit error rate (BER). An example of this is shown in Figure 7. Here, the signal levels of the main and diversity channels decreased while the cross-polar interference signal level increased. This level of interference was sufficient to close the eye and cause the BER to exceed 10^{-4} for 94 seconds. When both the 7.786 GHz and 7.765 GHz signal levels increased, the eye partially opened and the BER decreased. Errors continued until the end of the event, however.

Anomalous Frequency Dependence of Channel Attenuation

Figure 5 shows noticeably different cross-band but quite similar in-band channel attenuation responses during a melting layer event. In yet another event, the data show that the digital received signal level had different attenuation across its 40 MHz occupied bandwidth, as indicated by the adaptive equalizer slope, shown in Figure 4. In this case, the effect on the bit stream was again a considerable error rate, greater than 10^{-6} for 81 seconds. During this event, the cross-polar interference channel was not operating.

The hourly cumulative distributions of received signal level do not show anything that is very unusual. The cumulative distribution shown in Figure 7 is based on one hour (1500-1600) of the event shown in Figure 5. The slopes for the various frequency bands are similar but the median values of attenuation are different. The 4 GHz band appears to be affected less than either the 7 or 8 GHz bands.

DISCUSSION

Our observations indicate that the anomalous effects described above were generally associated with significant and sudden changes in meteorological parameters (temperature, wind direction, and wind speed) during the presence of the melting layer. These changes could have been caused by Pacific storms from the west creating strong turbulences as they moved inland into mountainous terrain. Such mechanisms are not, however, the subject of this paper.

The variability with frequency and polarization of the fading observed on this path suggests that some form of multipath propagation occurred during the presence of the melting layer. This is suggested for two reasons. Firstly, the occurrence of high BER during relatively shallow fades, as was observed, is typical of the usual multipath phenomena. Secondly, the melting layer is thought to be

TABLE 4 - Digital radio bit error performance

Date of Event	Bit Error Seconds BER > 0	BER > 10^{-6}	BER > 10^{-4}
1981-11-15	176	58	49
1982-01-23	605	181	94
1982-02-16	81	81	48

made of several distinct zones of snow in various stages of melting. Each zone has unique physical characteristic which depend on altitude, as reported by Nishitsuji and Matsumoto (7). This should create conditions capable of supporting multipath propagation.

Of major concern is the effect this anomalous fading has on digital radio transmission. The Trans-Canada Telephone System microwave design standard (8) allows 20 seconds of outage per year on this path, where outage is defined as the condition when the BER exceeds 10^{-4} for 175 ms. Table 4 summarizes the digital radio's bit error performance from November 1981 to March 1982. The cumulative outage duration exceeded the allowance set in the design standard even though fading never exceeded the 48 dB fade margin. Space diversity reception was not able to provide significant protection. In view of our observations, however, it appears that some form of frequency diversity might provide this protection.

REFERENCES

1. Watson, P.A., 1976, Proc. IEE, 123, 863-871.

2. Oomari, T., and Aoyagi, S., 1971, Elect. & Communic. in Jap., 54-B no. 9, 34-39.

3. Austin, P., 1964, "Observations of attenuation of 3 cm radiation by precipitation", Report of 1964 Conference in Radio Meteorology, Boulder, Colorado.

4. Van der Star, J., and Kharadly, M., 1981, Ann Telecommunic, 36 no. 1 & 2, 48-53.

5. Dissanayake, A.W., and McEwan, J.J., 1978, "Radar and attenuation properties of rain and bright band", IEEE Antennas and Propagation Conf. Proc., London, England.

6. DeWitte, G., 1978, "DRS-8: System Design of a Long Haul Digital Radio", National Telecommunications Conference, Birmingham, Alabama.

7. Nishitsuji, A., and Matsumoto, A., 1971, "The Character of Falling Snow", 19, Monograph Series of the Research Institute of Applied Electricity, Dapporo, Japan.

8. Roadhouse, R.S., et al., 1977, "The Trans-Canada Digital Radio Nework", International Conference on Communications, Chicago, Illinois.

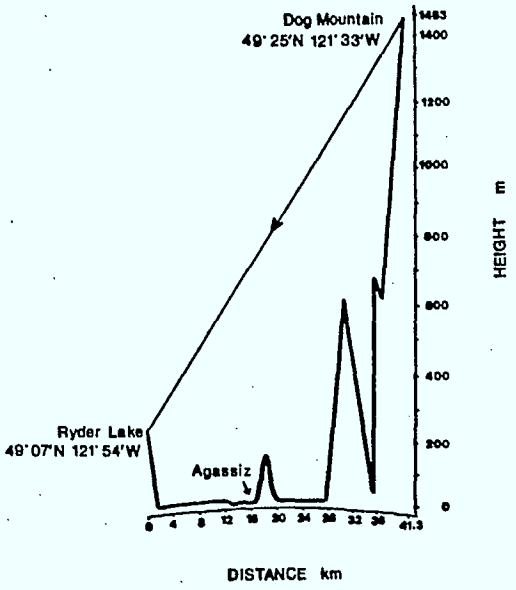

Figure 1 Path profile

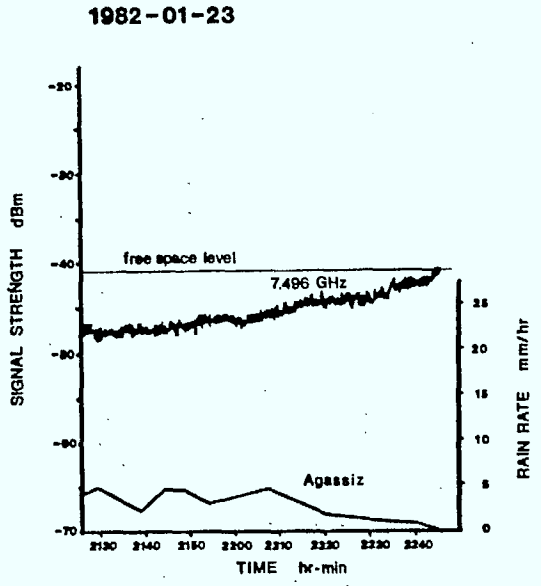

Figure 3 Example of excessive attenuation

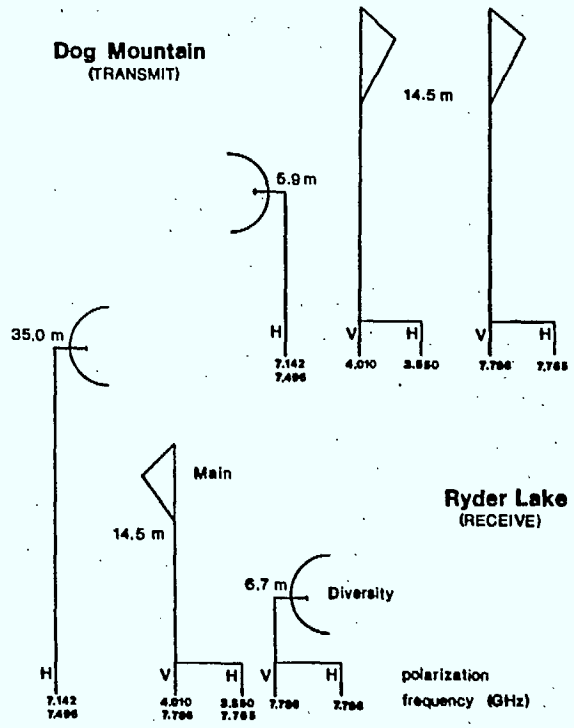

Figure 2 Antenna arrangement

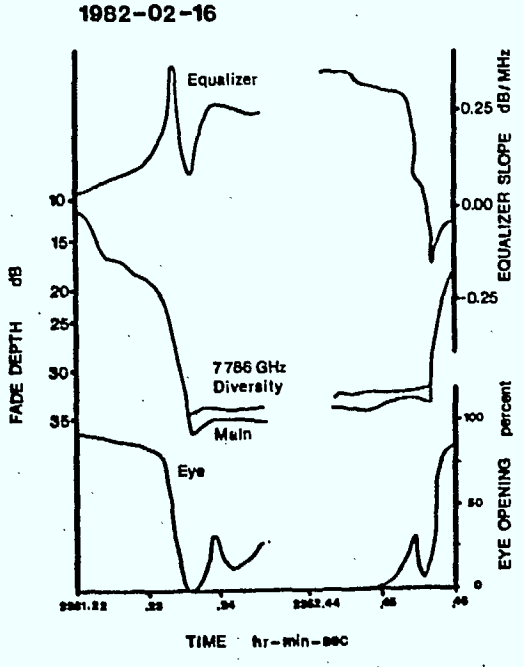

Figure 4 Example of abrupt changes in channel attenuation.

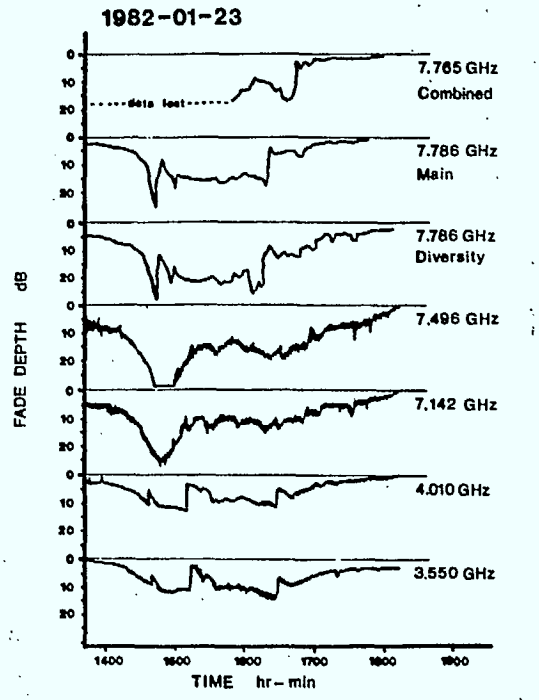

Figure 5 Propagation event of 23 January, 1982.

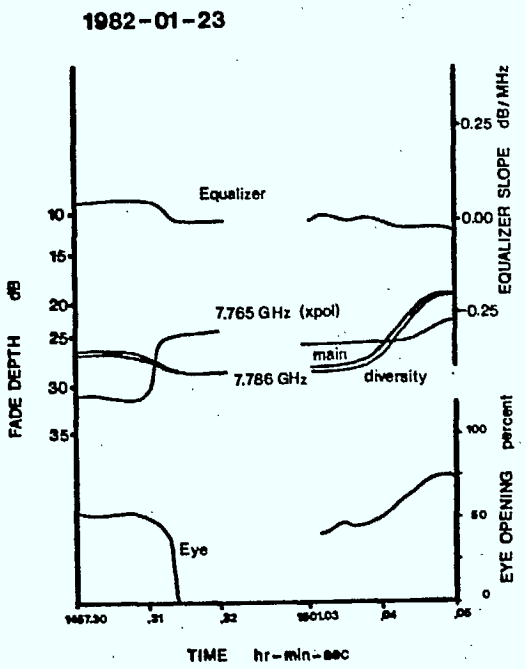

Figure 7 Example of polarization-dependent fading.

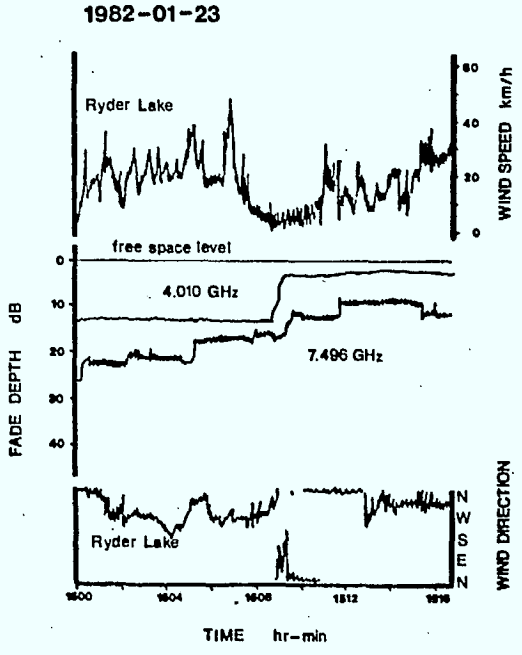

Figure 6 Anomalous fading at 4 and 7 GHz

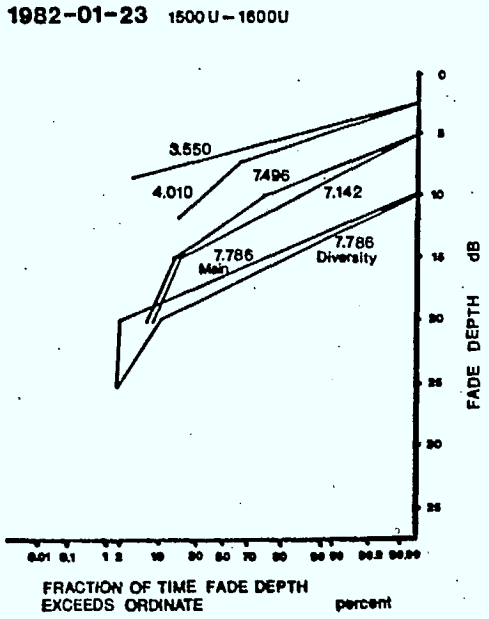

Figure 8 Cumulative distribution of received signal levels

Part II: Analysis of Multipath Fading Observations on Certain Microwave Paths in British Columbia

By: N. Owen, E. Lee and M. Kharadly

To be presented at the URSI Commission F 1983 Symposium on Wave Propagation and Remote Sensing, Louvain-La-Neuve, Belgium, 9-15 June, 1983.

ANALYSIS OF MULTIPATH FADING OBSERVATIONS ON CERTAIN MICROWAVE PATHS IN BRITISH COLUMBIA

N. Owen*, E. Lee† and M. Kharadly†

*British Columbia Telephone Company, Canada
†The University of British Columbia, Canada

ABSTRACT

The paper gives the results of measurements carried out on twelve microwave links throughout the Province of British Columbia, Canada. The links are representative of those in three of the five main topographic-climatic regions of this large province. The salient features of the microwave links on the paths are given. The observations are given in terms of worst-month multipath fading probability as a function of fade depth, the number of fading events and the variation of monthly fading time over the measurement period. The diurnal fading characteristics of several paths are also shown. The analysis involves comparisons of certain parameters derived from the observations with those given in the literature and generalized in the CCIR formula. An attempt is made to explain the observations in terms of terrain and climate.

Keywords: Multipath fading, Topographic-climatic conditions.

1. INTRODUCTION

In designing microwave links, one of the major considerations is estimating the probability of multipath fading (Ref. 1). In Canada, a typical design for a link, using frequency modulation and carrying analogue multiplex circuits, involves first ensuring an adequate free-space signal such that the circuit noise is within a prescribed limit. Then a calculation is made of the small percentage of the year during which high circuit noise is tolerated. It is this calculation that requires knowledge of fading, particularly multipath fading. In British Columbia (B.C.) we have found that, when modern radio equipment and careful link designs are used, the design point around the free-space level has been dominant, neglecting interference considerations.

Over the past few years, microwave links that use digital modulation have come into extensive use. Here, due to the nature of the modulation, the Bit Error Rate is of major concern and the designs are dominated by the need to maintain adequate signal to noise ratio, about 25 dB. This ratio is substantially smaller than that for analogue radio and consequently the small percentage of the year when the receive signal is faded becomes a major design consideration.

Digital radio links are observed to have high Bit Error Rates during relatively shallow multipath fades, usually of no consequence with analogue radio. To take this shallow fading into account in design requires knowledge of the probability of fading. It is also expected that further information, such as the number and duration of fading events, will be required as digital designs evolve.

It is thus evident that improved calculations of the overall probability of fading would be useful in obtaining more efficient designs.

Different investigators (Refs. 2-6) have proposed different parameters for the CCIR formula (Ref. 7) for various topographic - climatic regions. This formula shown as Eq. 1, gives the overall probability of tropospheric fading on paths without significant reflections.

$$Pr(W) = P_M \cdot K \cdot Q \cdot \frac{W}{Wo} \cdot f^B \cdot d^C \qquad (1)$$

where,

- Pr(W) : the overall probability of fading at power level W
- P_M : the probability that deep fading occurs
- K : the climatic factor
- Q : the terrain factor
- Wo : the free space power level
- f : the carrier frequency (GHz)
- d : the path length (km)
- B,C : suitable exponents.

This paper attempts to draw from data collected between July '79 and October '82 the parameters applicable to B.C. for the CCIR formula. British Columbia which is situated on the Pacific Coast of Canada, can be divided into five topographic - climatic regions and about 90% of the microwave links are distributed in three of them. Data acquisition systems were set up on some existing links in these regions in order to study propagation phenomena.

2. REGIONS AND MICROWAVE LINKS CONSIDERED

The B.C. terrain is essentially mountainous and its climate (Ref. 8) is mainly governed by the Coastal and Rocky Mountain ranges. The major air flow is westerly from the Pacific Ocean with an occasional Arctic air flow during winter. Most of the precipitation falls on the western side of mountain slopes.

The three regions of interest are the Coastal Mountains and Islands, the Interior Plateau and the Columbia Mountains and Southern Rockies. The first region is characterized by heavy precipitation especially in autumn and winter, mild winters and cool summers. The second region is much drier having warm summers and cold winters. Moreover, greater seasonal and diurnal temperature variations can be observed but the precipitation is quite evenly distributed throughout the year. The third

Table 1. Salient features of measured links

CLIMATIC REGION	LINK LABEL	SITE TX	SITE RX	ANT.HT.(m) TX	ANT.HT.(m) RX	FREQ.(GHz) PATH LEN.(Km)	TER.ROUGH.(m)+ MN.SLOPE (mrad)	COVERAGE & TERRAIN	DATA COLL. PERIOD	REC. TYPE
THE COASTAL MOUNTAINS & ISLANDS	A	Big Sicker 48° 51' 38" N 123° 45' 20" W	Vancouver 49° 16' 52" N 123° 07' 02" W	740	105	4.2 / 66.1	428 (96) / 9.6	60% water 40% trees	Jul 79 Oct 79	CHT CST
	B	Vancouver 49° 16' 52" N 123° 07' 02" W	Big Sicker 48° 51' 38" N 123° 45' 20" W	99	740	8.2 / 66.1	428 (96) / 9.6	60% water 40% trees	Jul 80 Oct 80	CHT CST
	C	Hope 49° 24' 35" N 121° 33' 28" W	Chilliwack 49° 06' 52" N 121° 54' 07" W	1489	282	7.8 / 41.4	719 (313) / 29.2	50% fields 50% trees on mtns.	Feb 81 Oct 82	CHT
	D	Blackwall 49° 06' 05" N 120° 45' 25" W	Hope 49° 24' 35" N 121° 33' 28" W	2028	1474	3.8 / 67.6	705 (408) / 8.2	trees on mtns.	Feb 81 May 82	CHT THD
THE INTERIOR PLATEAU (NORTH)	E	Firth 54° 48' 45" N 122° 46' 11" W	Tabor 53° 54' 44" N 122° 27' 01" W	1050	1253	7.5 / 102.3	415 (95) / 2.0	trees on rel. flat terrain	Jul 81 Oct 82	CHT THD
	F	McEwan 54° 24' 11" N 122° 29' 45" W	Tabor 53° 54' 44" N 122° 27' 01" W	1124	1262	3.8 / 45.7	463 (134) / 2.4	trees on rel. flat terrain	Jul 81 Oct 82	CHT
	G	Hixon 53° 28' 43" N 122° 38' 00" W	Tabor 53° 54' 44" N 122° 27' 01" W	843	1306	3.9 / 49.8	223 (133) / 9.3	trees on rel. flat terrain	Jul 81 Oct 82	CHT
	H	Prince George 53° 54' 54" N 122° 44' 52" W	Tabor 53° 54' 44" N 122° 27' 01" W	580	1274	11.5 / 19.6	229 (139) / 35.9	trees on rel. flat terrain	Jul 81 Oct 82	CHT
	I	Cluculz 53° 54' 15" N 123° 27' 25" W	Fraser 54° 01' 51" N 124° 37' 21" W	955	1160	7.2 & 7.5 (Ch.1) (Ch.2) / 77.8	303 (72) / 2.6	trees on rel. flat terrain	Apr 80 May 81	CHT high resol.
THE COLUMBIA MOUNTAINS & SOUTHERN ROCKIES	J	Creston 49° 05' 35" N 116° 22' 45" W	Salmo 49° 04' 18" N 117° 04' 56" W	2133	2179	4.1 / 51.4	1029 (541) / 0.4	trees on mtns.	Feb 82 Oct 82	CHT
	K	Rossland 49° 05' 35" N 117° 47' 50" W	Salmo 49° 04' 18" N 117° 04' 56" W	1280	2172	6.9 / 52.3	696 (415) / 17.2	trees on mtns.	Feb 82 Oct 82	CHT
	L	Santa Rosa 49° 01' 27" N 118° 03' 31" W	Salmo 49° 04' 18" N 117° 04' 56" W	1715	2182	4.1 / 71.6	878 (352) / 6.6	trees on mtns.	Feb 82 Oct 82	CHT THD

+The figure without bracket is the terrain roughness defined as the standard deviation of terrain elevation at 1 Km intervals about the mean slope of the path (excluding terminals) whereas the figure with brackets is the terrain roughness defined as the standard deviation of terrain elevations at 1 Km interval (excluding terminals) which will be used in the Extended Barnett parameters mentioned later (Ref. 7).

Quadrature partial response signalling (QPRS) modulation was used in links B,C, and FM modulation was used in all other links.

region is in general drier than the first and the precipitation on the windward slope brings moisture to the western side, leaving the valleys between the mountains semi-arid. This region has warm summers and cold winters with most precipitation occurring in winter. The geographical distribution of the links investigated and their salient features are shown in Figure 1 and Table 1, respectively.

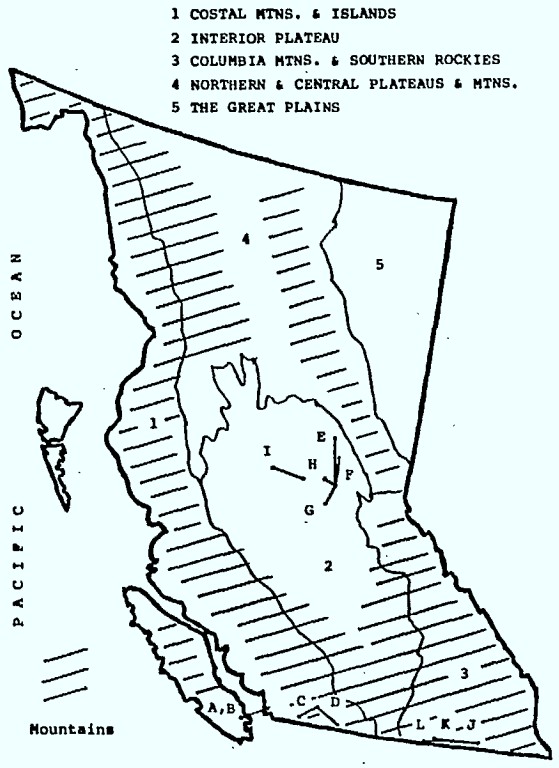

Figure 1. Distribution of microwave links investigated.

3. DATA ACQUISITION

The data reported are derived from recordings of the automatic gain control signal (AGC). The information obtained consists of the time below a given fade depth (relative to free space), the number of occurrences and the time of day of multipath fading.

Three data acqusition methods have been used. The one with the best time resolution (0.1 second) used magnetic tape cassettes (CST) and computer reconstruction of the data. The second method used a voltage threshold detector (THD) with four pre-set thresholds and a time resolution of 1 second. The third method was by chart recording (CHT) and had a time resolution of about 10 seconds except for link I (high resolution chart). Although the analysis of the data obtained by the chart recording method was laborious, it was considered invaluable in distinguishing fading conditions from other events. In order to obtain the best possible accuracy from the chart recordings, however, a comparison was made with the data collected by a threshold detector as detailed in the Appendix. The results of this comparison were utilized in the analysis of links C,F,G,H,J,K. It was also partially utilized for link E, as part of the worst month threshold detector data of this link was lost.

4. OBSERVATIONS AND ANALYSIS

A summary of the data is given in Table 2 which show the worst calendar month of multipath fading probability versus fade depth. The worst calendar month was determined using a -15 dB threshold for all links except A & B. For A & B a -20 dB threshold was used. Figure 2 compares the results from the measured data with those from various predic-

Table 2. Worst month multipath fading probability versus fade depth

LINK	FADE PROB. (X 10^{-6}) VS. FADE DEPTH (dB)							WORST MONTH
	-10	-15	-20	-25	-30	-35	-40	
A			961		155		15	Oct 79
B			352	78	21	4	0.7	Jul 80
C	45	12	2	2				Jul 82
D		38		8				Dec 81
E		1973	490	200		19		Sep 82
F	386	77	6					Sep 82
G	515	65	11	2	0.7	0.7		Sep 82
H	409	236	45	37		11	7	Jul 82
ICh.1	7675	553	119	29				Jul 80
Ch.2	2449	548	85	29				Sep 80
J	28	9	6	6			2	Feb 82
K	59	22	6					Oct 82
L	604		105		27	9		Oct 82

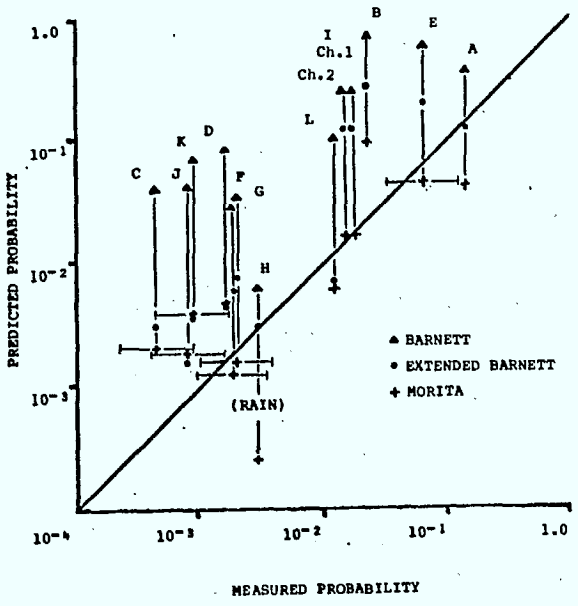

Figure 2. Worst calendar month multipath fading probability - predicted vs. measured.

tions for the worst calendar months. In plotting Figure 2, a slope of -10 dB per decade of probability for the measured data is assumed as in the CCIR formula. In cases where there was a scatter of data points, the -15 dB point was picked as a reference through which the -10 dB per decade line was passed.

The predicted results were obtained by employing parameters proposed by Barnett (Refs. 5,7) and Morita (Refs. 2,7). Since the terrain roughness, as used by Barnett, has an upper bound of 42 m, and this is exceeded by all our links, we have increased the upper bound to infinity and called the parameter thus obtained the Extended Barnett parameter, as indicated in the footnote of Table 1.

In Figure 2, if the measured and the predicted probabilities are the same, the point will fall on the 45° line. As we can see, the Morita prediction is nearest to the line, the Extended Barnett prediction is somewhat conservative whereas the Barnett prediction is overly conservative. Error bars are applied to links involving chart estimation (Appendix). The abnormally heavy fading in link H was due to heavy thundershower attenuation, as discussed in a later section.

Table 3. Number of events in worst month vs. fade depth

LINK	NO. OF EVENTS VS. FADE DEPTH (dB) -10	-15	-20	-25	-30	-35	-40
A			248		84		21
B+			117	48	16	5	
C	24	9	3	3			
D		3		2			
E		329	173	84		10	
F	74	10	3				
G	63	21	6	3	3	3	
ICh.1	117	37	14	7			
Ch.2	57	30	16	8			
J	15	3	3	3			3
K	15	6	3				
L	33		6		6	5	

+ Incomplete month

Table 4. Average fade duration in worst month vs. fade depth

LINK	AVERAGE FADE DURATION (SEC.) VS. FADE DEPTH (dB) -10	-15	-20	-25	-30	-35	-40
A			10.4		4.9		1.9
B+			4.9	2.8	1.9	1.6	
D		34.3		10.5			
ICh.1	175.7	40.1	22.7	11.1			
Ch.2	111.3	47.3	13.8	9.4			
L	49.0		47.0		12.0	4.8	

+ Incomplete month

Beside investigating the worst month fading probability, we have attempted to deduce from our measured data (Tables 3 and 4) the appropriate value of α_1 in Eq. 2 which gives the number of events and that of α_2 in Eq. 3 which gives the average fade duration. Eqs. 2 and 3 are given below (Ref. 7).

$$N^* = C_1 \cdot \left(\frac{W}{Wo}\right)^{\alpha_1} \cdot f^{\beta_1} \qquad (2)$$

$$\bar{t} = C_2 \cdot \left(\frac{W}{Wo}\right)^{\alpha_2} \cdot f^{\beta_2} \qquad (3)$$

where,

- N^* : the number of events at power level W in the worst month
- $\bar{t}$: the average fade duration at power level W
- C_1, C_2 : the proportionality constants
- Wo : the free space power level
- f : the carrier frequency (GHz)
- α_1, α_2 : the exponent parameters for power ratio W/Wo
- β_1, β_2 : the exponent parameters for frequency f.

The parameter α_1, can be obtained directly from Eq. 2 or indirectly from Eq. 3 through the relationship $\alpha_1 = 1 - \alpha_2$. We refer to data as "direct" when they are obtained from the links involving no chart estimation (A,B,D,I & L) and as "direct estimates" when they involve chart estimation (C,E,F,G,J & K) and as "indirect" when they are obtained from $\bar{t}$ of links (A,B,D,I & L). The values for α_1 concentrated in the 0.6 slot (0.6 - 0.69) as shown in Table 5 for these different types of data. It thus seems reasonable to suggest that $\alpha_1 = 0.67$ and hence $\alpha_2 = 0.33$ would be appropriate for application in B.C. These values are also the values applicable to Denmark (Ref. 7).

Table 5. The value distribution of α_1

DATA TYPE	α_1 0.2	0.3	0.4	0.5	0.6	0.7	0.8	0.9
Direct	1			2	1	1		1
Direct Estimates	1				3		1	1
Indirect		1	2		3			

Table 6 gives the information concerning monthly variation of fading. It is observed that the most active fading months are July to October. The year-to-year fading information is lacking and it is difficult to recognize any pattern. However, there is a tendency for fades to occur in the same period each year.

Other than on links, A, B and I, the yearly to worst fading month fading probability ratios (Table 6) lie between 1.0 and 1.7. (We assume that

Table 6. Monthly variation of fading and yearly to worst month fading probability ratio

LINK	FADE PROBABILITY ($\times 10^{-6}$) IN MONTHLY VARIATION J	F	M	A	M	J	J	A	S	O	N	D	YR.	YEARLY TO WORST MONTH	YEAR PERIOD
A							132	218	161	993			79	?	Jul 79 - Oct 79
B							352	204	246	318			80	?	Jul 80 - Oct 80
C		0	0	0	0	0	0	11	0	0	0	0	81	1.1	Oct 81 - Sep 82
	0	0	0	0	0	0.7	12	0	0	0			82		
D		0	0	0	15	0	0	0	0	0	0	40	81	1.4	Feb 81 - Jan 82
	0	0	0	0	0								82		
E							820	161	19	72	37	213	81	1.5	Nov 81 - Oct 82
	0	433	17	0	0	21	287	213	1900	38			82		
F							6	0	0	0	0	0	81	1.6	Nov 81 - Oct 82
	0	0	(0)	0	0	0	39	0	75	5			82		
G							0	0	0	0	0	0	81	1.2	Nov 81 - Oct 82
	0	0	(0)	0	6	0	6	0	65	0			82		
H							0	29	6	0	0	0	81	1.1	Nov 81 - Oct 82
	0	0	(0)	0	0	0	243	6	0	12			82		
ICh.1				161	9	72	572	(520)	310	284	4	0	80	3.8	Apr 80 - Mar 81
	233	0	0	32	21								81		
Ch.2				233	56	67	468	(520)	530	214	4	0	80	4.6	Apr 80 - Mar 81
	417	0	0	54	54								81		
J		6	0	0	0	0	0	o	0	4			82	1.7	Feb 82 - Oct 82
K		0	0	0	0	0	o	6	0	23			82	1.3	Feb 82 - Oct 82
L		0	0	0	0.8	0	11	0	0	(283)			82	1.0	Feb 82 - Oct 82

( ) : The data within brackets were obtained by interpolation.
Link C: The results exclude fading due to melting-layer conditions.
Link H: All the fading is probably precipitation-induced.

November to January are inactive months for links J,K,L.) This seems to suggest that for most links, we can take, conservatively, this ratio to be 2.0. Figure 3 shows the diurnal variation of fading. One can recognize two distinctive patterns. The links across dry and relatively flat terrain (E,F,G,I) have fading mostly around sunrise (0000-0800)+ as represented by link I. The links across water (A,B) or maybe even along a water body (C) have fading mostly around sunset (1600-2400) as represented by links B and C. The links across dry and mountainous terrain (D,J,K,L) have no general pattern.

5. TYPES OF MULTIPATH FADING OBSERVED

Multipath fading observed may be attributed to reflection or refraction from elevated or ground refractive layers, reflection from ground, from water or from atmospheric sheets (small refractive layers in the atmosphere). In some cases, multipath fading is associated with fog which produces a temperature inversion and a steep humidity gradient at the interface between the fog below and dry clear air above. The conditions that produce multipath fading in the various regions are discussed below in more detail.

+The number between brackets indicate Pacific Standard Time (PST)

5.1 Coastal links

The coastal links A & B experienced frequent multipath fading during the monitoring periods. Since any interfering signal due to water reflection was blocked by the intervening terrain, the occurrences of fading were due exclusively to the refractive layer(s). The three dominant mechanisms which could result in a refractive layer are sea breeze (1300-1900), offshore streaming (1700-0100) and advection of nocturnally - cooled air (2400-0900) as discussed in Refs. 9 and 10, and summarized below.

Sea breeze occurs during the afternoon along a coast when the land temperature is more than a few degrees higher than that of the sea, the warmer and drier air on land rises while the onshore breeze brings the cooler and more humid air from sea, undercutting the land air mass. Temperature inversion and steep humidity gradients will then produce a refractive layer at the air mass boundary. Under favourable conditions, the system can persist for several days.

Offshore streaming occurs around the evening when warm and dry air passes from land to the slightly cooler sea. The heat in the warm air is conducted downwards to the lower air layer in contact with the sea, while the moisture diffuses upwards from the sea surface to that layer. Hence, temperature

inversion and a steep humidity gradient exist between the bottom and upper air layers. A surface duct can then be formed extending some distance above the sea.

Advection of nocturnally-cooled air occurs around sunrise when the warmer sea and the cooler ground

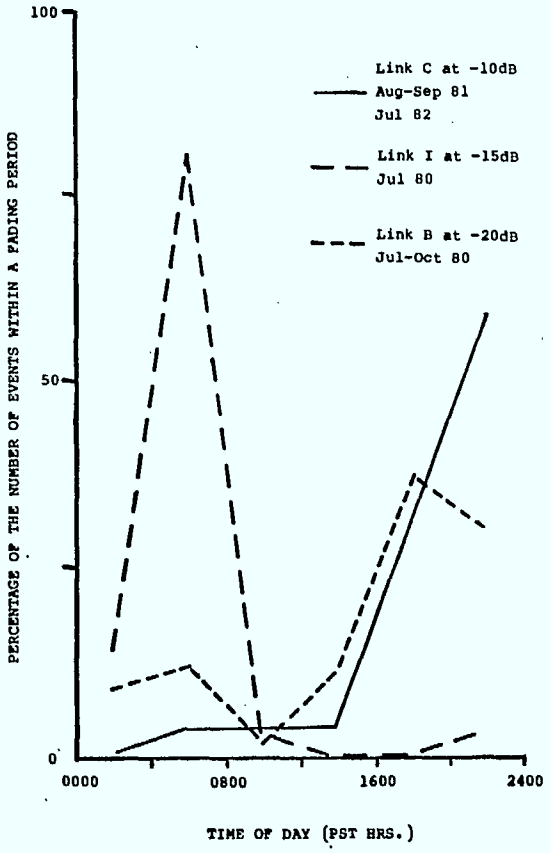

Figure 3. Diurnal variation of multipath fading

set up an offshore wind. This will carry the radiation inversion, and hence the refractive layer formed in the land air mass, to the sea. This radiation inversion is established when the heat absorbed in the ground during the day is allowed to radiate to the outer space through a clear sky, thus cooling the air layer near ground while the upper air temperature remains almost unchanged. However, once at sea, this temperature inversion will be upset since the warmer sea quickly modifies the temperature of the lower air layer.

From our observations shown in Figure 3, sea breeze and offshore streaming appear to be most pronounced in links A,B. Link C also displays similar diurnal variation characteristics, yet to a much lesser extent in terms of frequency of occurrence and fade depth. Noting that 50% of the terrain of link C consists of fields close to the Fraser River, one may expect that the local climatic conditions to be similar to those of the coast but on a smaller scale.

Rapid fading occurred on links A,B. This is thought to be due to multiple rays associated with slight changes in duct parameters if a duct is formed (Ref. 9). This is essentially the same as saying that it is due to reflection and/or refraction from one or more unstable refractive layers.

5.2 Plateau links

For the Interior Plateau region, it appears that the dominant mechanism for refractive layer formation is radiation inversion (Refs. 9,10) which occurs around sunrise (0000-0800). Refractive layer information was derived from daily (0400) radiosonde data at Prince George (15 km west of the Tabor receive site). Our observations show that of the thirteen fading events which occurred at the same time as radiosonde information, in eleven of them the top of the refractive layer was around the mean terminal height. We have assumed, in this analysis, that the layer followed the general contour of the path terrain. Calculations of the refractivity gradient, in N units per km, for those eleven events shows the gradients to be at -200 in one event, less than -150 in two events, between -150 and -100 in four events and between -100 and -80 in four events.

It is noteworthy that temperature inversion is common in this area. As an example, the radiosonde data showed that 85% of the July '81 days had temperature inversions at altitudes between 800 and 1500 m. This is the range of the transmitter and receiver heights and thus multipath fading is more likely to occur on such days. Moreover, the diurnal variation pattern (Figure 3) confirms the time of occurrence of radiation inversion.

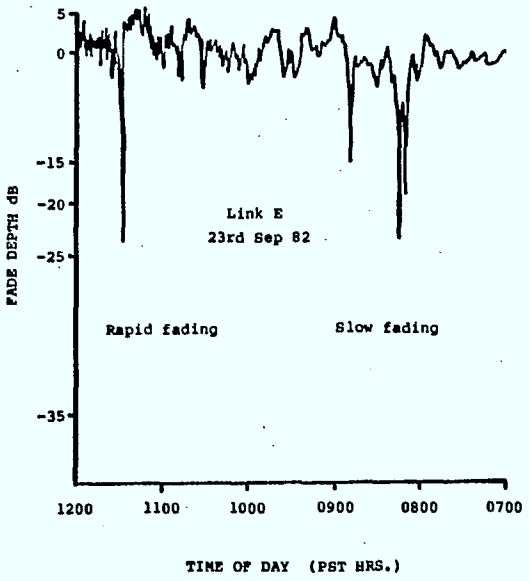

Figure 4. Rapid and slow multipath fadings

Slow multipath fading was sometimes observed (Figure 4) and is thought to be caused by reflection from relatively stable refractive layers. However, rapid (multi-ray) fading was more frequent and may be attributed to reflection and/or refraction from refractive layers and atmospheric sheets above the terminals (Figures 4 and 5). Furthermore, rapid scintillations (about 5 dB amplitude) also occurred without the presence of deep fading

(Figure 5). These are thought to be due to reflections from atmospheric sheets (Ref. 11). Scintillations begin about 1000 PST and lasted for several hours. It was observed that temperature inversion also started to break up at this time.

Figure 6 shows a general depression of the signal coupled with multipath fading. During this period ground fog patches were observed. Similar observations were previously reported (Ref. 11). A possible phenomenon which could explain this type of fading is discussed in Ref. 9. Briefly, radiation fog is formed beneath the radiation inversion (Ref. 12) and during the fog formation, the water vapour is condensed on the nuclei. This process reduces or even reverses the humidity gradient which could in turn result in subrefraction (Ref. 9) and possibly give rise to obstruction fading. The refractivity data taken approximately 6 hours after the event shown in Figure 6 shows that subrefractivity existed.

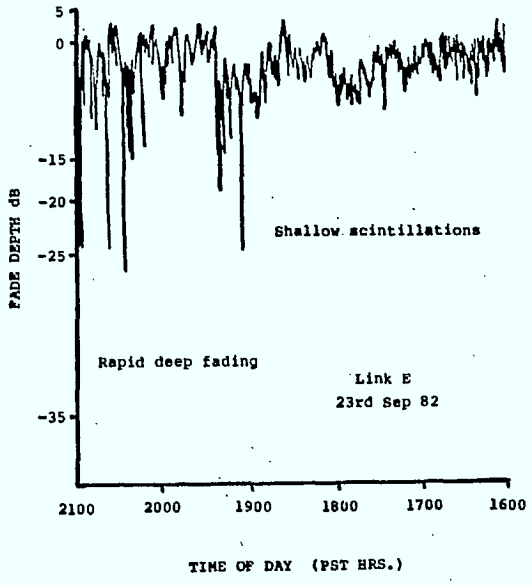

Figure 5. Rapid deep fading and shallow scintillations

Yet another type of fading, which resembles multipath fading (Figure 7), was observed on a very short link (link H, 19.6 km). Deep multipath fading is unlikely at 11 GHz on this link and this event was confirmed to be due to a heavy thundershower with a rainrate of 59 mm per hour.

5.3 Mountain links

The observations shown in Figure 2 indicate that the multipath fading probability for mountain links is comparable to that for plateau links. There is, however, no diurnal variation pattern (except for link C).

One of the possible mechanisms in this region would be refractive layer formation caused by temperature inversion and a steep humidity gradient across the interface of the upper, clear air and with radiation fog trapped in the valleys. This was the case in at least three fading events which occurred on links J, K and L during October 1982.

Rapid scintillations were also observed on the Columbia Mountains and Southern Rockies links (J,K,L). Although multipath fading is not a problem on link C, melting layer fading poses a severe problem (Refs. 14, 15). The worst month fading probability in 1982 was 0.86% (to -15 dB) and was all due to melting-layer conditions.

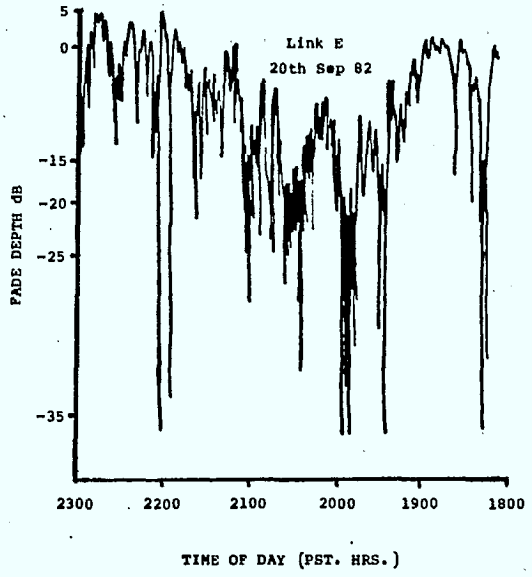

Figure 6. Obstruction fading coupled with multipath fading

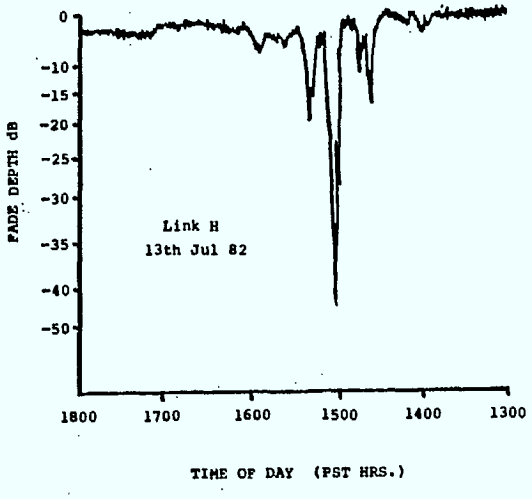

Figure 7. Rain-induced fading

6. CONCLUSIONS

We have presented and analyzed several multipath fading statistics for twelve microwave links in British Columbia. Our conclusions can be summarized as follows:

1. The Morita parameters, of the CCIR formula which describes multipath fading, are most appropriate for application to microwave links in B.C. The Extended Barnett parameters are more conservative and the Barnett parameters are overly conservative.

2. The exponent values in the expressions concerning the number of fading occurrences, N*, and the average fade duration, $\bar{t}$, be $\alpha_1 = 0.67$ and $\alpha_2 = 0.33$ respectively.

3. The most active fading period for multipath fading is July to October and the yearly to worst month fading ratio can be reasonably assumed as 2.0 for most links.

4. The peak of the diurnal multipath fading for links over, and perhaps along, a body of water is around the afternoon and at sunset. For plateau (or flat terrain), frequent fadings occur around sunrise and for most mountain links, there is no general pattern.

5. The dominant multipath mechanisms are (a) sea breeze, offshore streaming and advection of nocturnally-cooled air for coastal links, (b) radiation inversion for plateau links and (c) most likely trapped radiation fog in the valleys associated with upper, clear air for mountain links.

7. APPENDIX - CHART ESTIMATION

Many of the chart recordings had low resolution but presented no problem in the analysis of slow fading events where the down-stroke and up-stroke on the chart is separated by 1/2 mm which corresponds to 1 minute. However, this is not the case for rapid multipath fading where one or more events are so close together that they appear as one vertical line. In such cases, we estimated the duration by measuring the width of the line and then, dividing this width by an "Estimator". The Estimators corresponding to different widths are shown in Table A-1. The Estimators were obtained by comparing the chart and the threshold detector data of link E between 10th July - 11th August '81. The number of fade events corresponding to one line is estimated to be 3. This was also obtained from the comparison mentioned. The exact and estimated data are shown in Table A-2.

From the Exact/Estimated ratio (Table A-2) for fade duration and hence for the probability of multipath fading, the error is estimated to be from 0.5 to 2.0. The error bar in Figure 2 is set accordingly.

Table A-1. Estimator

MEASURED (MIN.)	ESTIMATOR
1/4	9
1/2	5
1-2	4
>3	3

Table A-2. Comparison of exact and estimated data

FADE DURATION (SEC.)			NO. OF EVENTS			FADE	
EXACT	ESTIM.	EXACT / ESTIM.	EXACT	ESTIM.	EXACT / ESTIM.	DEPTH (dB)	PERIOD
2319	1125	2.06	214	132	1.62	-18	10th Jul 82-
273	460	0.59	30	66	0.45	-23	11th Aug 82
132	196	0.67	25	48	0.52	-28	
22	26	0.85	14	27	0.52	-38	
900	1335	0.67	143	189	0.76	-15	22nd Sep 82-
301	530	0.57	74	105	0.70	-20	27th Sep 82

8. ACKNOWLEDGEMENTS

This work was supported by the Department of Communications, Ottawa, the British Columbia Telephone Company and the Natural Sciences and Engineering Research Council, Canada.

9. REFERENCES

1. CCIR, 1978, Effects of propagation on the design and operation of radio-relay systems, Question 25/9, CCIR XIVth Planary Assembly, Kyoto, 1978.

2. Morita, K., 1970, Prediction of Rayleigh fading occurrence probability of line-of-sight microwave links, Rev. Electr. Commun. Lab., V. 18, n. 11-12, pp. 810-822.

3. Blomquist, Å., and Norbury, J.R., 1978, Multipath effects on a terrestrial path, Influence of atmospheric conditions on electromagnetic wave propagation at frequencies above 10 GHz, EUROCOP-COST Final Rep. on Proj. 25/4, pp. 141-173, Comm. of the Eur. Communities, Brussels.

4. Doble, J.E., 1979, Predictions of multipath delays and frequency selective fading of digital links in UK. IEE Digest No. 1979/62, Nov.

5. Barnett, W.T., 1972, Multipath propagation at 4, 6 and 11 GHz, BSTJ, V. 51, n. 2.

6. Nadenenko, L.V., 1980, Kraschetu ustoychivosti signala na intervalakh radio-releynikh liniy pryamoy vidimosty (Calculation of signal stability in line-of-sight radio relay systems) NIIR Proc., n. 5.

7. CCIR, 1981, Propagation data required for line-of-sight radio-relay systems, Rep. 338-3 (MOD F) CCIR XVth Planary Assembly, Geneva, 1982.

8. Chilton, R., 1981, A Summary of Climatic regimes of British Columbia, Ministry of Envir., Assessment and Planning Division.

9. Jenkinson, G.F., 1967, Tropospheric Propagation: Radio - Meteorological Correlations over Bass Strait, Proc. I.R.E.E Aust. V. 28, n. 8, pp. 260-268.

10. Kerr, F.J., 1948, Radio super-refraction in the coastal regions of Australia, Aust. J. Sc. Res., Series A - Physical Sciences, V. 1, n. 4, pp. 443-463.

11. GTE Lenkurt Inc., 1975, Anomalous Propagation, GTE Lenkurt Demodulator, V. 24, n. 7, pp. 2-23.

12. Anderson, B.R., 1975, Weather in the West, Am. West Publ. Co., pp. 137-143.

13. Bello, P.A., DeRosa, J.K. Boardman, C.J., 1973, Line-of-sight wideband propagation CNR, Inc. Final Tech. Rep., May 1973, Sect. 3, p. 6.

14. Vander Star, J., Kharadly, M., 1980, Measurements of copolar attenuation through the bright band at 4 & 7 GHz, Proc. URSI Commission F Open Symposium, Lennoxville, Que., Canada, pp. 4.8.1-4.8.3, 1980.

15. Kharadly, M., et al., 1983, Observations of abnormal microwave propagation phenomena during melting layer conditions, 3rd Intl. Conf. on Ant. & Prop. ICAP 83, Norwich, UK, 12-15 April, 1983.

CACC / CCAC
38660

KHARADLY, M.
--Study of the propagation characteristics of certain ...

P
91
C655
K54
1983
v.5

DATE DUE
DATE DE RETOUR

LOWE-MARTIN No. 1137